Research Article | Vol. 12, No. 8 / 1 Aug 2022 / Optical Materials Express 3090
Optical Materials EXPRESS

Temperature-dependent photoluminescence of anatase Li-doped TiO_2 nanoparticles [Invited]

ANTONIO VÁZQUEZ-LÓPEZ,[1,2] ANA CREMADES,[1] AND DAVID MAESTRE[1,*]

[1]Department of Materials Physics, Faculty of Physics, Complutense University of Madrid, 28040 Madrid, Spain
[2]IMDEA Materials Institute, C/Eric Kandel, 2, Getafe, Madrid 28906, Spain
*dmaestre@ucm.es

Abstract: TiO_2 is currently one of the most employed material in photocatalysis and optoelectronic applications. By doping with different elements, tailored luminescent and optoelectronic properties can be obtained, which further enhances its applicability. The achievement of deeper knowledge and control on the recombination processes via light-metal doping engineering promises a wider use in optoelectronic applications. In this work, the luminescent properties of undoped and Li-doped anatase TiO_2 nanoparticles obtained by hydrolysis process are studied, by means of photoluminescence (PL) measurements from 10 K to room-temperature. TiO_2 presents a wide emission which covers the visible range, while Li-doping quenches the emission on the low visible region. By terms of time-resolved luminescence (TR-PL), lifetime of the recombination processes can be obtained, in which a decrease on lifetime values can be observed for the doped samples.

1. Introduction

Titanium dioxide (TiO_2) is currently one of the most suitable metal oxide semiconductors (MOs) due to its low toxicity, abundance, and low price, as well as to its photocatalytic and optoelectronic properties [1]. TiO_2 (titania) is widely used in photocatalysis and optoelectronic applications, as it possesses remarkable properties such as a high photoluminescence quantum yield, good electrical conductivity, wide bandgap, and high refractive index, among others. The applications of titania cover several fields in photonics as well, as it has been used in waveguides [2], optical resonators [3], photocatalysis [4], and solar cells [5], among others. In fact, the combination of titania with other compounds to assemble composites is a well-known practice in fields such as hybrid silicon solar cells [6], gas sensors, and thermoelectric materials [7]. Moreover, MOs are particularly regarded as interesting electron transport layers (ETL) due to the versatile processing conditions and electronic properties [8,9]. In the search of improved performance and novel applicability, further studies are required in the study of titania nanostructures.

TiO_2 has different polymorphs, rutile, anatase and brookite, among which anatase and rutile are the most popular ones [5]. In particular, anatase TiO_2, which has an indirect band gap of 3.2 eV at room temperature, is a metastable phase, considered to exhibit better photocatalytic activity than rutile, the stable phase [1], although mixed phases can also show improved photocatalytic performance anatase properties are strongly linked to the morphology, dimensions, composition, and surface-to-volume ratio. A common approach to tailor its optoelectronic response consists in doping TiO_2 with different elements [2,4,10,11] which can increase optical gain in different wavelengths [2], or improve the electrical conductivity, as well as the photocatalytic performance [4,12]. Several dopants have shown to play a role on tailoring the luminescence properties, mostly transition metals as Cu- [13], Fe-[14] Mn-[15], Cr-[16] or rare earths-[17], by adding novel states in the bandgap or alter the radiative recombination paths. Among the light-metal dopants, Lithium is recently arising increasing attention as a potential dopant for anatase, as it

#465710 https://doi.org/10.1364/OME.465710
Journal © 2022 Received 1 Jun 2022; revised 1 Jul 2022; accepted 2 Jul 2022; published 18 Jul 2022

Optical Materials EXPRESS

has shown superior photocatalytic activity [12,18] and enhanced electrical conductivity, which improves the overall performance in Lithium ion batteries (LiBs) [10,11], leading as well to enhanced stabilization of anatase phase against rutile [11,19]. However, the radiative processes involved in the Li doped TiO_2 luminescence still need to be deeply investigated in order to exploit the applicability of this material, as less works have been reported in this field despite to potential interest of the Li doped titania nanostructures.

Although, great research has been conducted on the synthesis and characterization of titania nanoparticles so far, the mechanisms related to the excitation and relaxation processes in titania are not fully understood yet [1,20], and requires of further studies. The limitation on the charge mobility in titania can be a limiting factor for applications, hence necessary research has to be conducted to shed light in this topic. Among the different characterization techniques which allow this study, the most common one is the steady-state photoluminescence (PL) spectroscopy at room temperature (RT) and low temperature, down to 4K, as at RT some contributions are difficult to observe and analyze [16].

Recently, time-resolved PL (TR-PL) has been employed to resolve the lifetime of photo-generated electrons and holes in anatase, providing insights on the dominant decay mechanisms [1,20–23], the study of which can lead to improved knowledge of the photocatalytic and luminescent behaviour. TR-PL has been employed to study anatase layers [20], mixed anatase-rutile phases [23], or nanoparticles, focusing on the effect of the pH [1] however fewer works consider the effect of dopants by means of TR-PL, despite their great influence in the luminescence. In fact, the work from Dozzi of et al. is one of the very few studies using TR-PL for doped anatase, in their case F-doped anatase [24]. Currently, the formation of MOs-heterojunction to improve ETL layers are gaining interest, where significant PL quenching confirms superior electron extraction ability [9], in that sense doping-MOs is also a potential approach.

Herein, optical and electric properties from Li-doped TiO_2 nanoparticles have been studied by diverse techniques. The luminescent-dependence of Li-doped TiO_2 nanoparticles has been analyzed by means of the temperature-dependent PL-measurements and time-resolved photoluminescence (TR-PL) spectra at temperatures down to 10 K. The kinetics of the luminescence bands as a function of the Li doping and the temperature are discussed based on the non-radiative transitions obtained from the Arrhenius analysis of the PL intensity and lifetime decay.

2. Experimental section

TiO_2 and Li-doped TiO_2 nanostructures were synthesized following a hydrolysis method, as reported in a previous work [11]. To summarize, stoichiometric amounts of the precursors were mixed into a beaker and then distilled water was used to induce the hydrolysis at room temperature. Then, the product was centrifuged with distilled water until reaching neutral pH and then dried in an oven at 50°C during 12 h. Finally, the product was annealed at 250°C during 24 h. Three different samples were analyzed in this case: undoped TiO_2 and Li-doped TiO_2 with Li in two weight percentages, respective to the precursor weight (20 and 30%) labeled as TiO_2, TiO_2:$Li_{0.2}$ and TiO_2:$Li_{0.3}$. The Li doped samples showed a Li content of 0.50% at. (TiO_2:$Li_{0.2}$) and 0.65% at (TiO_2:$Li_{0.3}$), as confirmed by inductively coupled plasma optical emission spectroscopy (ICP-OES) measurements [11].

The microstructural analysis was performed using a transmission electron microscope (TEM) JEM 1400 plus JEOL. The morphological characterization was carried out by Raman spectroscopy at room temperature using a Horiba Jobin-Yvon LabRam Hr800 (Horiba, Kyoto, Japan) with a continuous wave He-Cd laser ($\lambda = 325$ nm). The laser was focused onto the sample surface using a 40× objective (numerical aperture = 0.5, Thorlabs LMU-40X-NUV), which led to a laser spot diameter around 1 μm for the UV. The scattered light was collected with the same objective and dispersed with a grating of 2400 L/mm and finally acquired with an air-cooled CCD detector Synapse.

Optical Materials EXPRESS

Particles were pressed into pellets for the following measurements. Synchrotron radiation X-ray photoelectron (XPS) spectroscopy have been performed at the CNR Beamline for Advanced dichroism (BACH) at the Elettra synchrotron facility in Trieste, Italy. The photoelectron spectra were acquired using a Scienta R3000 electron energy analyzer. All core-levels and valence band spectra were recorded with a total energy resolution of 180 meV. For those measurements, the samples were prepared as pellets. Li 1s was calibrated to Ti 3s (62.5 eV) [11] while the surveys was calibrated using C 1s core level at 284.6 eV.

Steady state Photoluminescence (PL) and time resolved photoluminescence (TR-PL) measurements were acquired with an Edinburgh Instruments FLS1000 system, equipped with double monochromator and a cryogenic setup to operate from 10 K up to RT with a variable light source from a 450 W ozone-free Xenon lamp for steady-state. Lifetime measurements were obtained using a pulsed LED with excitation wavelength of $\lambda_{LED} = 256.8$ nm and ~1 ns pulse width as excitation source and with a repetition rate of the pulses of 5 MHz.

For the electrical characterization, Hall effect measurements were performed at room temperature using a current of 10 nA on a Hall Ecopia AMP55T with four gold probes and using HMS-7000 control electronics. Contacts were prepared with silver paste (RS Silver Conductive 186-3600).

3. Discussion

3.1. Structural characterization of undoped and Li-doped TiO_2 nanoparticles

Due to the high yield of the synthesis method, large quantity of TiO_2 nanoparticles can be obtained, for both the Li-doped and undoped samples. Prior to the luminescence study, the morphological, structural, compositional, and electrical properties of the samples were analyzed. In our previous report [11] the presence of Li in the samples was assessed by ICP-OES analysis, which indicated values in the range of 0.5–0.65 at. %. XRD measurements confirmed the only presence of anatase for all the synthesized samples, no rutile or other crystalline phases were observed. The synthesized particles present averaged sizes between 6–7 nm, as observed from TEM images, being slightly bigger the particles doped with Li. All particles present a round shape and good size-homogeneity, as observed in the TEM image form TiO_2:$Li_{0.3}$ (Fig. 1(a)), being similar for the rest of the samples [11]. The corresponding SAED pattern (inset in Fig. 1(a)), shows only the expected diffraction planes for anatase TiO_2, further assuring the phase homogeneity of the samples.

The Raman spectra for each sample (TiO_2, TiO_2:$Li_{0.2}$ and TiO_2:$Li_{0.3}$) are shown in Fig. 1(b). Vibrational modes from rutile are not observed in the Raman spectra despite the UV laser employed as excitation source. Only Raman peaks corresponding to anatase active vibrational modes [11,25] are identified for all the samples. These modes are, for the undoped sample, positioned at 152 cm^{-1} (E_g), 203 cm^{-1} (E_g), 404 cm^{-1} (E_g), 521 cm^{-1} (B_{1g} +A_{1g}), and 632 cm^{-1} (E_g), respectively. Some of the Raman modes are slightly shifted towards lower wavenumber, as well as showing a wider FWHM as well, due to the small size of the synthesized particles. A wider contribution is observed around 800−840 cm^{-1}, commonly related to B_{1g} overtone scattering [25], although its origin is still under debate. Variations in the relative intensity as well as the positions of the Raman peaks can be appreciated as a function of the amount of dopant, as observed in Fig. 1(b), which can be attributed to defects and stoichiometry changes in the samples due to the lithium insertion. The most notable change in the Li-doped samples is the quenching of the E_g mode, a vibration mode which is associated with symmetric bending vibrations of O-Ti-O groups. This mode is sensitive to changes in the stoichiometry of the material and the presence of oxygen vacancies, most likely created due to the charge imbalance induced by Lithium doping, hence larger oxygen deficiency is observed in the Li doped samples.

To analyze the presence of lithium in the samples, XPS measurements were also conducted on the TiO_2 materials pressed into pellets [11]. From the XPS surveys acquired at 253 eV, shown in

Optical Materials EXPRESS

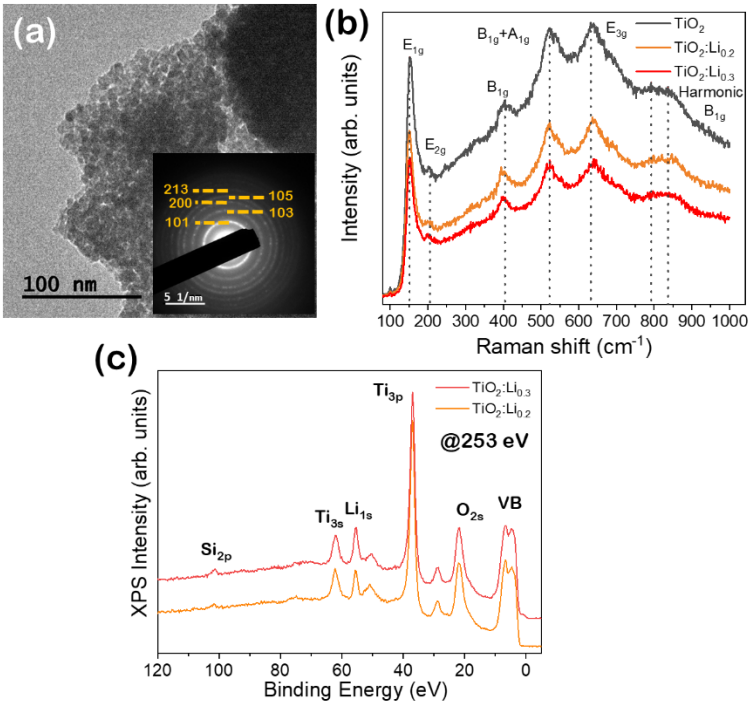

Fig. 1. (a) TEM image of TiO_2:$Li_{0.3}$ nanoparticles. Inset shows the corresponding SAED pattern. (b) Raman spectra of TiO_2, TiO_2:$Li_{0.2}$ and TiO_2:$Li_{0.3}$ samples and (c) XPS survey of TiO_2:$Li_{0.2}$ and TiO_2:$Li_{0.3}$ samples acquired with a beam energy of 253 eV.

Fig. 1(c), the core level from Li 1s can be clearly observed at 55.4 and 55.5 eV for TiO_2:$Li_{0.2}$ and TiO_2:$Li_{0.3}$, respectively, thus confirming Li doping. No Ti^{3+} contribution was observed in the samples, which indicates that the lithium incorporation is mediated by the formation of mostly oxygen vacancies.

Overall, the structural characterization confirms the high crystallinity of the synthesized nanomaterial as well as the phase homogeneity, being anatase the only titania phase observed.

By means of Hall effect, the electrical conductivity of the samples was obtained at room temperature. The conductivity values are shown in Table 1. All the samples exhibit n-type conductivity, as expected, and conductivity values in the range of 10^{-6} to 10^{-7} S cm^{-1}. As observed, Li doped samples are more conductive than undoped TiO_2. The enhancement in the conductivity could be due to changes in particle size, porosity, and defects promoted during doping. Nonetheless, effects related to the grain size and the structure of the pressed pellet could also affect the conductivity [26]. In this case, the increased oxygen deficiency observed in the Li doped TiO_2, in agreement with Raman measurements, could also be related to the increased conductivity.

Table 1. Variation in the conductivity of the undoped and Li doped TiO_2 nanoparticles.

Sample	σ (S·cm^{-1})
TiO_2	$(1.2 \pm 0.1)\cdot10^{-7}$
TiO_2:$Li_{0.2}$	$(8.3 \pm 0.9)\cdot10^{-7}$
TiO_2:$Li_{0.3}$	$(2.2 \pm 0.1)\cdot10^{-6}$

Optical Materials EXPRESS

3.2. Temperature dependent photoluminescence

The study of the variation of the PL signal as a function of the temperature allows to get insights in the thermally activated processes and defect-states involved in the radiative and non-radiative recombination paths in the samples under study. Figure 2 shows the series of the PL spectra acquired under the excitation obtained from a Xe discharge lamp monochromated at 290 nm (4.3 eV), which is larger than the anatase optical bandgap (~387.5 nm, 3.2 eV). In this work, series of spectra were acquired over a variable range of temperatures, from 10 K to 300 K (RT), in steps of 10 K. Previous reports have pointed out the possible transition from anatase to rutile during UV laser irradiation [27], thus minimum exposure time was employed in this case in order to avoid possible phase transition.

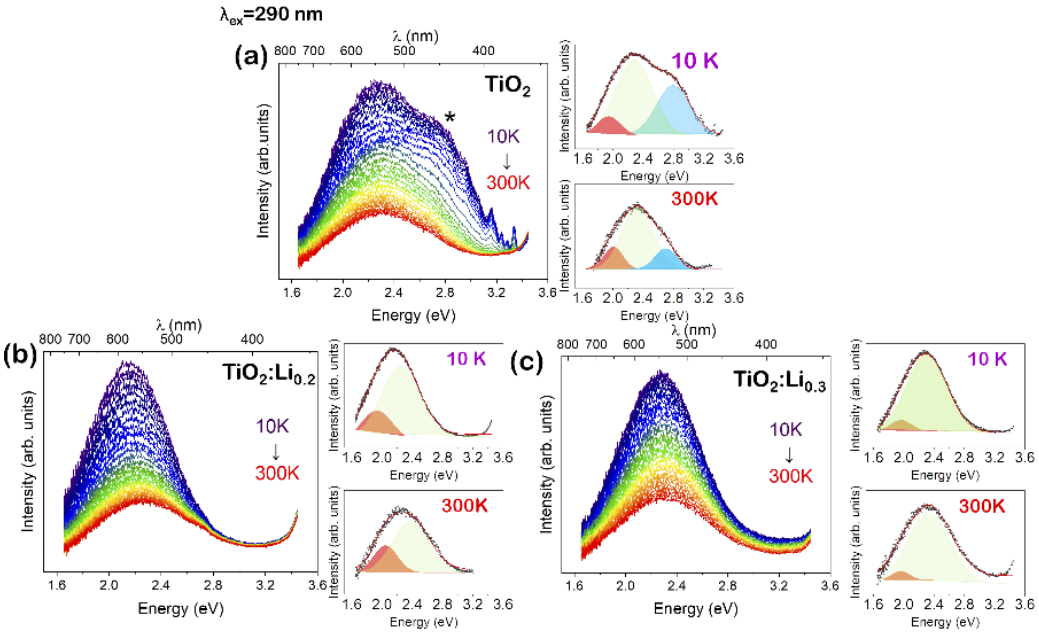

Fig. 2. Photoluminescence (PL) spectra as a function of the temperature obtained under 290 nm excitation between 10 and 300 K in steps of 10 K for the samples (a) TiO_2 (b) TiO_2:$Li_{0.2}$ and (c) TiO_2:$Li_{0.3}$. The corresponding deconvolution to Gaussian functions of the PL spectra at 10 or 300 K are also included beside each Figure.

The luminescence from all the samples shows a clear temperature dependence following a decrease in the PL total intensity as the temperature rises from 10 K to RT. Similar temperature dependent behavior in the PL signal has been commonly reported for other semiconductors, owing to the increase in the probability of the non-radiative recombination paths as the temperature rises, among other factors. In order to analyze the temperature dependent PL signal, deconvolutions to Gaussian functions of representative spectra acquired at 10 K and 300 K were also performed for each sample, as shown in Fig. 2. In this case, three main contributions are required to obtain a good fit for undoped TiO_2 (1.9, 2.3 and 2.9 eV), while only two contributions at 1.9 eV and 2.3 eV are necessary for achieving a good fit for the Li doped samples.

PL spectra of anatase TiO_2 is commonly attributed to different physical origins, such as oxygen vacancies, self-trapped excitons (STEs), surface states or localized excitons [1,14,20,21,28,29]. The first two contributions are commonly referred to as red band (1.9 eV) and green band (2.3 eV), associated with oxygen deficiency-related defects [1,11,22,28]. In particular, the green band involves recombination of electrons in the conduction band or shallow traps with holes

Optical Materials EXPRESS

trapped in deep defect states, while the red band is usually related to recombination of electrons in deep traps with holes in the valence band. Besides, the relative intensity of the red band (1.9 eV), related to sub-surface oxygen vacancies, is lower as the content of Li increases. On the other hand, the emission 2.9 eV, marked with an asterisk in Fig. 2(a), is commonly related to self-trapped excitons (STE) in anatase TiO_2 [16]. This STE-band, which is only observed in undoped TiO_2, starts to be noticeable at temperatures below 150 K, as at higher temperatures STE de-trapping is promoted. The absence of the STE-related emission (2.9 eV) in the Li-doped samples, together with the increase in the relative intensity of the green emission (2.3 eV) can be associated with the defect structure introduced by Li doping, which enhances the formation of oxygen vacancies (V_O) defects, in agreement with Raman spectroscopy (Fig. 1(b)). At low temperature, below 100 K, narrow and weak emissions can be also observed around 3.0 eV only for the undoped TiO_2 sample, which can arise as a result of strong exciton–phonon interaction in TiO_2 under high-power UV irradiation [16], or the presence of excitons bounded to shallow defects. Furthermore, PL spectra from all the samples show a bathochromic redshift as the temperature decreases, being this effect most noticeable for TiO_2:$Li_{0.2}$.

Fig S1 shows the PL spectra from the undoped and Li doped samples acquired at a fixed temperature (either 10 K or RT). At RT all the samples show a similar emission (Fig S1(b)), however at 10 K, differences can be distinguished in the PL spectra as a function of the Li doping (Fig. S1(a)), being the PL signal from undoped TiO_2 wider and more complex, due to the presence of the STE-band. Despite the fact that all the samples show similar luminescence intensity, the highest PL intensity at 10 K is observed for TiO_2:$Li_{0.2}$, while TiO_2:$Li_{0.3}$ shows the lowest PL, which could indicate that low-Li content may slightly enhance photoluminescence radiative recombination processes. Differences with the Li content on the PL intensity can be observed in Fig. S1(c). Some other studies [30] report variable Li incorporation as a function of the amount of dopant, being Li more favorable to occupy interstitial positions at low doping conditions and also substitutional positions at higher doping doses, which can also alter the luminescent behaviour.

In the analysis of the temperature dependent PL, competitive processes between radiative recombination paths and thermally activated non-radiative recombinations are usually considered. Actually, the PL intensity quenching with increasing temperature is a well-known defect-related phenomenon which has been explained for several semiconductors, including anatase TiO_2, following different models, which mostly rely on the empirical Arrhenius expression [20], for which in anatase is usually given as:

$$I^{PL}(T) = \frac{I_0^{PL}}{1 + A \cdot exp\left(-\frac{E_A}{k_B \cdot T}\right) + B \cdot exp\left(-\frac{E_B}{k_B \cdot T}\right)} \quad (1)$$

In Eq. (1), $I^{PL}(T)$ represents the emission intensity as a function of the temperature, I_0^{PL} denotes the PL emission intensity in the limit of low temperatures, A and B are coefficients A=$\tau_R/(\tau_A + \tau_{A\downarrow})$ given by the ratio of the luminescent radiative lifetime and the inverse transition probabilities of the non-luminiscent states and the luminiscent ones, and the ground states, k_B is Boltzmann's constant, and E_A and E_B are an activation energy for thermal quenching process. Depending on the model, these E_A and E_B could be ascribed to some features occurring during the luminescence process that involve defect-related centers.

Figure 3(a) shows the PL intensity integrated over the whole emission represented versus $1/k_BT$, where a clear decrease in the PL signal is observed as the temperature raises, mainly at temperatures above 100 K. The PL quenching with the temperature is similar for the three samples under study, although slight differences in the decay profiles can be observed as a function of the Li doping. In all the cases, at least, two activation processes with energies E_A and E_B are required, as indicated in Eq. (1), to account the experimental results and to obtain a

Optical Materials EXPRESS

good fitting to the model, in which a ground state, a radiative state, and two thermally activated non-radiative channels are considered [20]. The fitting parameters corresponding to each sample are shown in Table 2. Comparable PL quenching as the temperature rises is observed for all the samples, therefore only slight variations are expected in the values of A, B and E_A and E_B, in agreement with the estimated values depicted in Table 2. This could indicate that probably two processes with similar origin should be considered in the PL emission for all the samples, probably involving intragap defect-states.

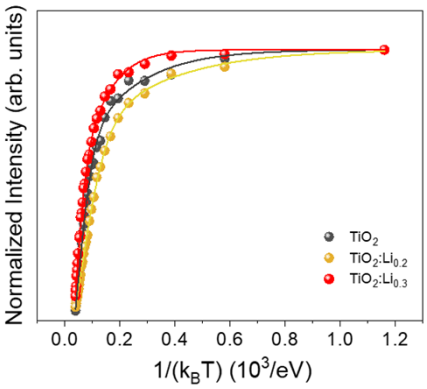

Fig. 3. Photoluminescence (PL) emission intensity of the total intensity of the different samples (TiO_2 TiO_2:$Li_{0.2}$ and TiO_2:$Li_{0.3}$) as a function of $1/k_BT$ obtained under 290 nm excitation wavelength between 10 and 300 K each 10 K. The solid line are the fitting results from Eq. (1)

Table 2. Fitting parameters of experimental data which shows the activation energies obtained from Arrhenius fitting of the PL curves vs. $1/k_BT$ using an excitation wavelength of $\lambda_{ex} = 290$ nm

Sample	A	E_A[meV]	B	E_B[meV]
TiO_2	0.4 ± 0.1	5.7 ± 0.9	7.3 ± 0.6	37.9 ± 2.2
TiO_2:$Li_{0.2}$	0.4 ± 0.1	3.7 ± 0.4	4.1 ± 0.1	22.2 ± 0.7
TiO_2:$Li_{0.3}$	0.8 ± 0.1	11.9 ± 0.9	11.5 ± 1.5	58.4 ± 3.8

From Table 2 we can observe that for all the samples the activation energy E_B is around six times larger than E_A, while the order of magnitude of both activation energies, in the meV range, is in good agreement with previous reports [20]. Furthermore, the activation E_A is below the room temperature ($k_BT = 25.9$ meV) for all the cases, while E_B is higher for TiO_2:$Li_{0.3}$ showing values over k_BT also for undoped TiO_2, therefore being more difficult to be thermally activated. Based on the activation energies of the thermally activated non-radiative processes, the quantum efficiency of the radiative recombinations is low at RT for all the samples thus leading to lower PL signal as the temperature rises.

Considering the good fitting of the temperature-dependent PL signal, only slight variations in the recombination channels are induced by Li doping in anatase TiO_2. Apart from the quenching of both the STE-emission at 2.9 eV and the narrow emissions around 3 eV, Li doping promotes the formation of oxygen vacancies related defects which leads to the prevalence of the green-band emission at 2.3 eV.

Optical Materials EXPRESS

3.3. Time-resolved photoluminescence

TR-PL measurements have been carried out for all the samples at 10 K. This technique provides very valuable information on the luminescence mechanism as it allows to observe the PL decay after an excitation pulse, which can be employed to calculate the lifetime of the diverse recombination process. The results are shown in Fig. 4. In this study, the instrument response (IR) after stimulation, displayed as a black line in Fig. 4, has been removed to discern the information given by our sample and subtract any noise from the instrument.

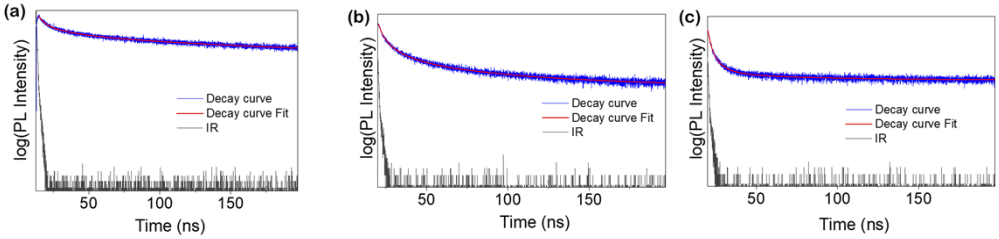

Fig. 4. Decay time fit (red solid line) corresponding to the curves (blue) obtained at 10 K for (a) TiO_2 (b) TiO_2:$Li_{0.2}$ and (c) TiO_2:$Li_{0.3}$ in which the instrument response (IR, black solid line) has been considered.

Among the different functions which can be employed to fit the decay exponential times proposed in the literature [24] in our case the best fitting results were obtained with three exponential decay components, according to Eq. (2).

$$I(t) = B_1 e^{\left(-\frac{t}{\tau_1}\right)} + B_2 e^{\left(-\frac{t}{\tau_2}\right)} + B_3 e^{\left(-\frac{t}{\tau_3}\right)} \tag{2}$$

where B_i ($i = 1,\ 2,\ 3$) and τ_i correspond to the amplitude and lifetimes, respectively, of the three luminescent components. The parameters estimated from the fitting of the TR-PL results to Eq. (2) are shown in Table 3.

This multi-exponential decay can be associated with multiple trapping and de-trapping of carriers. In this case, the dynamics of the photo-excited carriers lie in the ns range for all the samples, in agreement with some other reports also considering three main components. However, it can be observed that two processes (τ_1, τ_2) are faster while the third one (τ_3) is slower. The two fastest components can be ascribed to exciton recombinations, while the third component can be attributed to surface processes involving intragap defect-states [24]. In fact, in Ref. [29] three components with τ_1~2.5 ns, τ_2~25 ns and τ_3~300 ns were also reported, in agreement with the order of magnitude from our observations (Table 3). In our case, lifetimes values are always lower for the Li doped samples, actually the lowest values are estimated for the sample TiO_2:$Li_{0.3}$, as shown in Table 3. In this case, the photoexcited charge carriers can rapidly recombine by radiative or non-radiative paths in the ns range, which can be associated with the PL decay as the temperature increase up to RT, as observed in this work. Considering that all the samples consist in anatase with low dimensions and high surface to volume ratio, surface trapped stated should be considered in the analysis, probably related to oxygen deficiency. Furthermore, the lower lifetime values observed for the doped samples could indicate an enhancement of the charge carriers recombination by Li doping.

Optical Materials EXPRESS

Table 3. Exponential fitting results of the PL decay.

Sample	τ_1[ns]	τ_2[ns]	τ_3[ns]
TiO_2	4.9	21.8	222.89
TiO_2:$Li_{0.2}$	3.4	14.4	88.1
TiO_2:$Li_{0.3}$	3.1	8.4	64.2

4. Conclusions

In this work, undoped and Li doped TiO_2 nanoparticles synthesized by hydrolysis have been analyzed in order to assess the variations induced by Li doping. Only slight morphological changes have been observed in the nanoparticles, which exhibit dimensions around 6–7 nm. However, variations in the electrical and optical properties as well as in the oxygen deficiency have been promoted as a function of Li doping. Hall effect results show that Li doping enhances the electrical conductivity in the nanoparticles, while some of the Raman modes from the Li doped samples exhibit a low quenching which can be related to the higher presence of defects and oxygen vacancies. Regarding the luminescence of the analyzed samples, variations have been observed as a function of the temperature and the presence of Li. Undoped TiO_2 presents a wide emission in the visible range which can be ascribed to three main contributions, a red band (1.9 eV), a green band (2.3 eV), and a band related with the presence of STE (2.9 eV). For the lithium doped samples, the STE-related band is completely quenched, which indicates a different defect structure and variable recombination process dynamics promoted by Li doping. Despite extensive study regarding this material, some of its most fundamental luminescent mechanisms have not been fully understood yet. In the search of novel insights in this field, techniques such as steady photoluminescence as a function of temperature and Time-Resolved photoluminescence (TR-PL) can lead to improved knowledge of the thermally activated processes and defect-states involved in the radiative and non-radiative recombination paths. In this work, the temperature dependent PL shows a quenching of the luminescence as the temperature raises, which has been fitted to a model including two thermally-activated non-radiative channels. The estimated activation energy of the thermal quenching processes, in the range of meV, are lower for the Li doped samples. The PL decay and the study of lifetime values, by means of TR-PL, indicates a tri-exponential model where the presence of Li favors the fast recombination of luminescent surface trapping sites, in the ns range.

Funding. Spanish Ministry of Innovation, Science, and Technology and the Spanish Ministry of Economy (RTI2018-097195-B-I00).

Acknowledgments. Authors thanks Dr. Igor Píš and Dr. Silvia Nappini from BACH beamline at Elettra-Sincrotrone Trieste S.C.P.A. for their valuable help during XPS measurements and analysis. Authors thank Dr. J. Ramírez-Castellanos for supervision during the nanoparticles synthesis process.

Disclosures. The authors declare no conflicts of interest

Data availability. Data underlying the results presented in this paper are not publicly available at this time but may be obtained from the authors upon reasonable request.

Supplemental document. See Supplement 1 for supporting content.

References

1. R. Brüninghoff, K. Wenderich, J. P. Korterik, B. T. Mei, G. Mul, and A. Huijser, "Time-dependent photoluminescence of nanostructured anatase TiO_2 and the role of bulk and surface processes," J. Phys. Chem. C **123**(43), 26653–26661 (2019).
2. F. B. Segerink, I. Hegeman, M. Dijkstra, S. M. Garcia-Blanco, and W. Lee, "Development of low-loss TiO_2 waveguides," Opt. Express **28**(5), 5982–5990 (2020).
3. C. C. Evans, E. Mazur, I. B. Burgess, J. T. Choy, J. D. B. Bradley, M. Lončar, and P. B. Deotare, "Integrated TiO_2 resonators for visible photonics," Opt. Lett. **37**(4), 539–541 (2012).

Optical Materials EXPRESS

4. Y. Wang, M. Zu, X. Zhou, H. Lin, F. Peng, and S. Zhang, "Designing efficient TiO_2-based photoelectrocatalysis systems for chemical engineering and sensing," Chem. Eng. J. **381**, 122605 (2020).
5. Y. Zhang, Z. Jiang, J. Huang, L. Y. Lim, W. Li, J. Deng, D. Gong, Y. Tang, Y. Lai, and Z. Chen, "Titanate and titania nanostructured materials for environmental and energy applications: A review," RSC Adv. **5**(97), 79479–79510 (2015).
6. A. Vázquez-López, A. Yaseen, D. Maestre, J. Ramírez-Castellanos, S. Z. Karazhanov, E. S. Marstein, and A. Cremades, "Improved silicon surface passivation by hybrid composites formed by PEDOT:PSS with anatase TiO_2 nanoparticles," Mater. Lett. **271**, 127802 (2020).
7. A. Vázquez-López, J. García-Alonso, S. Nahirniak, J. Bartolomé, J. Ramírez-Castellanos, D. Maestre Varea, B. Saruhan, and A. Cremades, "Synthesis and characterization of semiconducting oxide nanoparticles and hybrid composites with energy-related applications," Oxide-based Mater. Devices XIII 12002F, (2022).
8. J. Zhao, L. Wei, J. Liu, P. Wang, Z. Liu, C. Jia, and J. Li, "A sintering-free, nanocrystalline tin oxide electron selective layer for organometal perovskite solar cells," Sci. China Mater. **60**(3), 208–216 (2017).
9. M. Thambidurai, S. Foo, K. M. Muhammed Salim, P. C. Harikesh, A. Bruno, N. F. Jamaludin, S. Lie, N. Mathews, and C. Dang, "Improved photovoltaic performance of triple-cation mixed-halide perovskite solar cells with binary trivalent metals incorporated into the titanium dioxide electron transport layer," J. Mater. Chem. C **7**(17), 5028–5036 (2019).
10. A. Vázquez-López, M. García-Carrión, E. Hall, A. Yaseen, I. Kalafat, M. Taeño, J. Zhu, X. Zhang, E. Arici, O. S. Taskin, D. Maestre, E. Nogales, P. Hidalgo, J. Ramírez-Castellanos, B. Méndez, N. Yuca, S. Karazhanov, E. S. Marstein, and A. Cremades, "Hybrid materials and nanoparticles for hybrid silicon solar cells and Li-ion batteries," J. Energy Power Technol. **03**(02), 1 (2020).
11. A. Vázquez-López, D. Maestre, R. Martínez-Casado, J. Ramírez-Castellanos, I. Píš, S. Nappini, and A. Cremades, "Unravelling the role of lithium and nickel doping on the defect structure and phase transition of anatase TiO_2 nanoparticles: Chemical routes to materials," J. Mater. Sci. **57**(14), 7191–7207 (2022).
12. T. N. Ravishankar, G. Nagaraju, and J. Dupont, "Photocatalytic activity of Li-doped TiO_2 nanoparticles: Synthesis via ionic liquid-assisted hydrothermal route," Mater. Res. Bull. **78**, 103–111 (2016).
13. B. Choudhury, M. Dey, and A. Choudhury, "Shallow and deep trap emission and luminescence quenching of TiO_2 nanoparticles on Cu doping," Appl. Nanosci. **4**(4), 499–506 (2014).
14. J. Zhang, X. Chen, Y. Shen, Y. Li, Z. Hu, and J. Chu, "Synthesis, surface morphology, and photoluminescence properties of anatase iron-doped titanium dioxide nano-crystalline films," Phys. Chem. Chem. Phys. **13**(28), 13096–13105 (2011).
15. B. Choudhury and A. Choudhury, "Tailoring luminescence properties of TiO_2 nanoparticles by Mn doping," J. Lumin. **136**, 339–346 (2013).
16. L. Kernazhitsky, V. Shymanovska, T. Gavrilko, V. Naumov, L. Fedorenko, V. Kshnyakin, and J. Baran, "Photoluminescence of Cr-doped TiO2 induced by intense UV laser excitation," J. Lumin. **166**, 253–258 (2015).
17. I. Cacciotti, A. Bianco, G. Pezzotti, and G. Gusmano, "Synthesis, thermal behaviour and luminescence properties of rare earth-doped titania nanofibers," Chem. Eng. J. **166**(2), 751–764 (2011).
18. Y. Liang, K. Su, L. Cao, and Z. Li, "Lithium doped TiO_2 as catalysts for the transesterification of bisphenol-A with dimethyl carbonate," Mol. Catal. **465**(2019), 16–23 (2019).
19. D. A. H. Hanaor and C. C. Sorrell, "Review of the anatase to rutile phase transformation," J. Mater. Sci. **46**(4), 855–874 (2011).
20. M. Gallart, T. Cottineau, B. Hönerlage, V. Keller, N. Keller, and P. Gilliot, "Temperature dependent photoluminescence of anatase and rutile TiO_2 single crystals: Polaron and self-trapped exciton formation," J. Appl. Phys. **124**(13), 133104 (2018).
21. L. Cavigli, F. Bogani, and A. Vinattieri, "Volume versus surface-mediated recombination in anatase nanoparticles," J. Appl. Phys **106**(5), 053516 (2009).
22. M. Watanabe, S. Sasaki, and T. Hayashi, "Time-resolved study of photoluminescence in anatase TiO_2," J. Lumin. **87-89**, 1234–1236 (2000).
23. X. Wang, S. Shen, Z. Feng, and C. Li, "Time-resolved photoluminescence of anatase/rutile TiO_2 phase junction revealing charge separation dynamics," Chinese J. Catal. **37**(12), 2059–2068 (2016).
24. M. Vittoria Dozzi, B. Ohtani, G. Valentini, and E. Selli, "Fluorine-doped TiO_2 materials: photocatalytic activity vs time-resolved photoluminescence," J. Phys. Chem. C **117**(48), 25586–25595 (2013).
25. L. Miao, S. Tanemura, S. Toh, K. Kaneko, and M. Tanemura, "Fabrication, characterization and Raman study of anatase-TiO_2 nanorods by a heating-sol–gel template process," J. Cryst. Growth **264**(1-3), 246–252 (2004).
26. J. Y. Yang, W. S. Li, H. Li, Y. Sun, R. F. Dou, C. M. Xiong, L. He, and J. C. Nie, "Grain size dependence of electrical and optical properties in Nb-doped anatase TiO_2," Appl. Phys. Lett. **95**(21), 213105 (2009).
27. E. Dauksta, A. Medvids, P. Onufrijevs, M. Shimomura, Y. Fukuda, and K. Murakami, "Laser-induced crystalline phase transition from rutile to anatase of niobium doped TiO_2," Curr. Appl. Phys. **19**(3), 351–355 (2019).
28. D. K. Pallotti, L. Passoni, P. Maddalena, F. Di Fonzo, and S. Lettieri, "Photoluminescence mechanisms in anatase and rutile TiO_2," J. Phys. Chem. C **121**(16), 9011–9021 (2017).
29. I. Sildos, A. Suisalu, J. Aarik, T. Sekiya, and S. Kurita, "Self-trapped exciton emission in crystalline anatase," J. Lumin. **87-89**, 290–292 (2000).

Optical Materials EXPRESS

30. A. Vázquez-López, D. Maestre, J. Ramírez-Castellanos, J. M. González-Calbet, I. Pis, S. Nappini, N. Yuca, and A. Cremades, "Influence of doping and controlled Sn charge state on the properties and performance of SnO_2 nanoparticles as anodes in Li-ion batteries," J. Phys. Chem. C **124**(34), 18490–18501 (2020).